Computation and visualization of photonic quasicrystal spectra via Bloch's theorem

Alejandro W. Rodriguez,[1,*] Alexander P. McCauley,[1] Yehuda Avniel,[2] and Steven G. Johnson[3]
[1]*Department of Physics, Massachusetts Institute of Technology, Cambridge, Massachusetts 02139, USA*
[2]*Research Laboratory of Electronics, Department of Electrical Engineering and Computer Science, Massachusetts Institute of Technology, Cambridge, Massachusetts 02139, USA*
[3]*Department of Mathematics, Massachusetts Institute of Technology, Cambridge, Massachusetts 02139, USA*
(Received 13 November 2007; published 7 March 2008)

Previous methods for determining photonic quasicrystal (PQC) spectra have relied on the use of large supercells to compute the eigenfrequencies and/or local density of states. In this paper, we present a method by which the energy spectrum and the eigenstates of a PQC can be obtained by solving Maxwell's equations in higher dimensions for any PQC defined by the standard cut-and-project construction, to which a generalization of Bloch's theorem applies. In addition, we demonstrate how one can compute band structures with defect states in the same higher-dimensional superspace. As a proof of concept, these general ideas are demonstrated for the simple case of one-dimensional quasicrystals, which can also be solved by simple transfer-matrix techniques.

DOI: 10.1103/PhysRevB.77.104201 PACS number(s): 71.23.Ft, 42.70.Qs

I. INTRODUCTION

We propose a computational method to solve for the spectra and eigenstates of quasicrystalline electromagnetic structures by directly solving a periodic eigenproblem in a higher-dimensional lattice. Such photonic quasicrystals (PQCs) have a number of unique properties compared to ordinary periodic structures,[1–23] especially in two or three dimensions where they can have greater rotational symmetry and, therefore, offer some hope of complete photonic band gaps with lower index contrast[6,24–26] than the roughly 2:1 contrast currently required for periodic structures.[27] However, the study of two- and three-dimensional photonic quasicrystals has been hampered by the computational difficulty of modeling aperiodic structures, which has previously required large "supercell" calculations that capture only a portion of the infinite aperiodic lattice. Our method, in contrast, captures the entire infinite aperiodic structure in a single higher-dimensional unit cell, and we believe that this approach will ultimately be much more computationally tractable for two- and three-dimensional quasicrystals. The idea that many quasicrystals can be constructed by an irrational slice of a higher-dimensional lattice is well known,[28–30] and, in fact, is the most common formulation of quasicrystals in two and three dimensions,[31–33] but the possibility of direct numerical calculations within the higher-dimensional space seems to have been little explored outside of some tight-binding calculations in quantum systems.[34,35] As a proof of concept, we demonstrate a first implementation of the technique applied to one-dimensional quasicrystals, such as the well-known Fibonacci structure. Not only can we reproduce the spectrum from transfer-matrix calculations, but we also show that the higher-dimensional picture provides an interesting way to visualize the eigenmodes and compute defect states in the infinite aperiodic structure.

There have been several previous numerical approaches to simulating quasicrystal structures in electromagnetism and quantum mechanics. In one dimension, a typical quasicrystal is an aperiodic sequence of two or more materials, determined either by a slice of a higher-dimensional lattice[29] or by some "string concatenation" rule.[28] In either case, efficient 2×2 transfer-matrix methods are available that allow one to quickly compute the transmission spectra and density of states for supercells consisting of many thousands of layers.[36,37] Two- and three-dimensional quasicrystals are almost always defined as an irrational slice (i.e., incommensurate Miller indices) of a higher-dimensional lattice; for example, the famous Penrose tiling can be viewed as a two-dimensional slice of a five-dimensional cubic lattice or of a four-dimensional root lattice A_4.[30] In such cases, supercell computations of a finite portion of the infinite aperiodic structure (or a rational approximant thereof[29,36]) require slower numerical methods, most commonly finite-difference time-domain (FDTD) simulations[13,19,38] or plane wave expansions.[39,40] Unfortunately, these methods become very expensive for large supercells, nearly prohibitively so for three-dimensional quasicrystals—there have been experiments for three-dimensional (3D) PQCs,[32,33] but as yet few theoretical predictions.[41,42] With FDTD methods, for example, the PQC local density of states is typically integrated in a Monte Carlo fashion via random sources or initial conditions,[8,11,23] but many simulations are required to sample all possible modes in a large supercell. Also, the finite domain of a supercell becomes even more significant in higher dimensions, where a tractable supercell is necessarily smaller, as there can be localized states[13,17,19,23] whose presence is dependent on the particular region of the PQC considered. Our method of computing the spectrum directly in the higher-dimensional unit cell, on the other hand, requires no supercell to capture the infinite aperiodic structure—it uniformly samples (up to a finite resolution) every possible supercell of the infinite quasicrystal, rather than any particular subsection. The influence of finite resolution on the convergence of the spectrum can be systematically understood: one is not "missing" any part of the quasicrystal, so much as resolving the entire quasicrystal with lower resolution.

The structure of this paper is as follows: In Sec. II, we review the "cut-and-project" method for defining a PQC as a slice of a higher-dimensional lattice, followed in Sec. III by a

description of our computational method in the higher-dimensional lattice. There, we describe the extension of Maxwell's equations to higher dimensions and also describe its solution in terms of a higher-dimensional Bloch plane wave expansion. As a proof of concept, we present a sequence of one-dimensional examples in Sec. IV. First, we compare results for a one-dimensional "Fibonacci sequence" with standard one-dimensional transfer-matrix techniques. Second, as mentioned above, we demonstrate how one can use the same technique to study defects in the quasicrystal, as demonstrated in the one-dimensional "Fibonacci" example. Finally, we demonstrate the ease with which one can construct and explore different quasicrystals by continuously varying the cut angle.

II. QUASICRYSTALS VIA CUT-AND-PROJECT

Given a periodic lattice, any lower-dimensional cross section of that lattice may be either periodic or quasiperiodic, depending on the angle of the cross section. For example, the periodic two-dimensional (2D) cross sections of a 3D crystal are the lattice planes, defined in crystallography by integer Miller indices. If the Miller indices have irrational ratios, on the other hand, the cross section is aperiodic but still has long-range order because of the underlying higher-dimensional periodicity. This is what is known as a cut-and-project method of defining a quasicrystalline structure: as a slice of a periodic structure in a higher-dimensional "superspace."[28,29] (For a thorough discussion of quasicrystals via cut-and-project, see Ref. 28.) Cut-and-project defines a specific class of quasicrystals; equivalently, and more abstractly, cut-and-project corresponds to structures whose Fourier transform has support spanned by a finite number of reciprocal basis vectors (the projection of the reciprocal lattice vectors from higher dimensions).[28,31] This class includes most commonly considered quasicrystals in two or three dimensions, including the Penrose tiling[30] and the 2D Fibonacci quasicrystal,[43] as well as many one-dimensional quasicrystals including a one-dimensional (1D) Fibonacci structure.

For example, consider the Fibonacci PQC in one dimension formed from two materials $\varepsilon_A=4.84$ and $\varepsilon_B=2.56$ in layers of thickness A and B, respectively, similar to a recent experimental structure.[7] The Fibonacci structure S is then defined by the limit $n\to\infty$ of the string-concatenation rule $S_n=S_{n-2}S_{n-1}$ with starting strings $S_0=B$ and $S_1=A$,[7] generating a sequence $BABAABABABAABA\ldots$. In the case where B/A is the golden ratio $\tau=(1+\sqrt{5})/2$, exactly the same structure can be generated by a slice of a two-dimensional lattice as depicted in Fig. 1.[28] The slice is at an angle ϕ with an irrational slope $\tan\phi=1/\tau$, and the unit cell of the 2D lattice is an $A\times A$ square at an angle ϕ in a square lattice with period $(A+B)\sin\phi=a$. Because the slope is irrational, the offset or intercept of the slice is unimportant: any slice at an angle ϕ intercepts the unit cell at infinitely many points, filling it densely.

For thickness ratios $B/A\neq\tau$, the Fibonacci structure cannot be constructed by cut-and-project, and, in general, string-concatenation rules can produce a different range of structures (such as the Thue-Morse PQC[44]) than cut-and-project. This is partly a question of definition—some authors reserve the term "quasicrystal" for cut-and-project structures.[30] In any case, cut-and-project includes a wide variety of aperiodic structures, including most of the structures that have been proposed in two or three dimensions (where they can be designed to have n-fold rotational symmetry for any n), and are the class of quasicrystals that we consider in this paper.

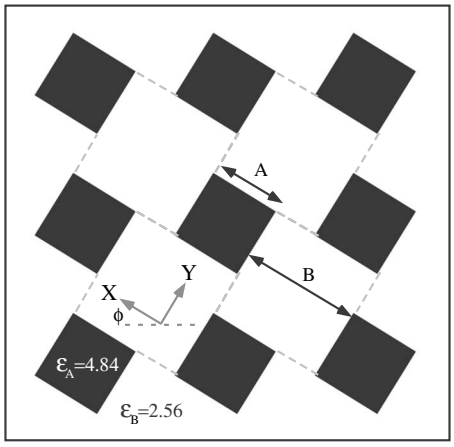

FIG. 1. Unit cell of the Fibonacci superspace dielectric. The physical dielectric is obtained by taking a slice at an angle $\tan\phi=\tau$. Black and white are the dielectric constants of the structure factor material and air, chosen to be $\varepsilon=4.84$ and $\varepsilon=2.56$, respectively.

In general, let $d\leqslant 3$ be the number of physical dimensions of a quasicrystal structure generated by a d-dimensional "slice" of an n-dimensional periodic structure ($n>d$). Denote this slice by X (the physical space) with coordinates $\mathbf{x}\in\mathbb{R}^d$, and denote the remaining $n-d$ coordinates by $\mathbf{y}\in\mathbb{R}^{n-d}$ in the "unphysical" space Y (so that the total n-dimensional superspace is $Z=X\oplus Y$). The primitive lattice vectors $\mathbf{R}_i\in Z$ define the orientation of the lattice with respect to the slice (rather than vice versa), with corresponding primitive reciprocal vectors $\mathbf{G}_i$ defined by the usual $\mathbf{R}_i\cdot\mathbf{G}_j=2\pi\delta_{ij}$.[28] (The concept of an "irrational slice" is commonly used in the quasicrystal literature. However, a general definition of what is meant by an irrational slice seems difficult to find, and less evident in dimensions $d>2$. A more precise definition of irrational slice in general dimensions and a proof that it is dense in the unit cell is given in the Appendix.)

The physical dielectric function $\varepsilon(\mathbf{x})$ is then constructed by starting with a periodic dielectric function $\varepsilon(\mathbf{x},\mathbf{y})$ in the superspace and evaluating it at a fixed $\mathbf{y}$ (forming the slice). Because an irrational slice is dense in the unit cell of the superspace,[28] it does not matter what value of $\mathbf{y}$ one chooses, as discussed below. In principle, one could define the unit cell of ε in the superspace to be any arbitrary n-dimensional function, but in practice, it is common to "decorate" the higher-dimension unit cell with extrusions of familiar d-dimensional objects.[28,30] More precisely, cut-and-project commonly refers to constructions where a set of lattice points within a finite window of the cut plane is projected onto the cut plane, and this is equivalent to a simple cut

where objects at the lattice points are extruded in the y direction by the window width.[28] In particular, the extrusion window is commonly an inverted projection (shadow) of the unit cell onto the y directions,[28] although this is not the case for the Fibonacci construction of Fig. 1.

(Note that the higher-dimensional lattice need not be hypercubic. For example, the Penrose tiling can be expressed as a two-dimensional slice of either a five-dimensional hypercubic lattice or of a nonorthogonal four-dimensional root lattice A_4.[30] For computational purposes, the lower the dimensionality, the better.)

III. COMPUTATIONS IN HIGHER DIMENSIONS

Although the cut-and-project technique is a standard way to *define* the quasicrystal structure, previous computational studies of photonic quasicrystals then proceeded to simulate the resulting structure only in the projected (d-dimensional) physical space. Instead, it is possible to extend Maxwell's equations into the periodic n-dimensional superspace, where Bloch's theorem applies to simplify the computation. By looking at only the unit cell in n dimensions, one can capture the infinite d-dimensional quasicrystal. Our development of this technique was inspired by earlier research on analogous electronic quasicrystals that applied a tight-binding method in two dimensions to compute the spectrum of a one-dimensional electronic quasicrystal.[34,35]

Let us start with Maxwell's equations in the physical space X for the quasicrystal $\varepsilon(\mathbf{x},\mathbf{y})$ at some fixed $\mathbf{y}$ (that is, $\mathbf{y}$ is viewed as a parameter, not a coordinate). Maxwell's equations can be written as an eigenproblem for the harmonic modes $\mathbf{H}(\mathbf{x},\mathbf{y})e^{-i\omega t}$,[45] where again $\mathbf{y}$ appears as a parameter:

$$\nabla_{\mathbf{x}} \times \frac{1}{\varepsilon(\mathbf{x},\mathbf{y})} \nabla_{\mathbf{x}} \times \mathbf{H} = \left(\frac{\omega}{c}\right)^2 \mathbf{H}, \tag{1}$$

where $\nabla_{\mathbf{x}}\times$ denotes the curl with respect to the $\mathbf{x}$ coordinates. Assuming that the structure is quasicrystalline, i.e., that X is an irrational slice of the periodic superspace Z, then ω should not depend on $\mathbf{y}$.[34] The reason is that $\mathbf{y}$ only determines the offset of the "initial" slice of the unit cell (for $\mathbf{x}=0$), but as we reviewed above, the slice (considered in all copies of the unit cell) fills the unit cell densely. Therefore, any change of $\mathbf{y}$ can be undone, to arbitrary accuracy, merely by offsetting $\mathbf{x}$ to a different copy of the unit cell. An offset of $\mathbf{x}$ does not change the eigenvalues ω, although, of course, it offsets the eigenfunctions $\mathbf{H}$.

The fact that ω is independent of $\mathbf{y}$ allows us to reinterpret Eq. (1), without actually changing anything: we can think of $\mathbf{y}$ as a coordinate rather than a parameter, and the operator on the left-hand side as an operator in d-dimensional space. Note that $\mathbf{H}$ is still a three-component vector field, and $\nabla_{\mathbf{x}}\times$ is still the ordinary curl operator along the $\mathbf{x}$ directions, so this is not so much a higher-dimensional version of Maxwell's equations as an extension of the unmodified ordinary Maxwell's equations into a higher-dimensional parameter space. The $\mathbf{y}$ coordinate appears in the operator only through ε. Because ω is independent of $\mathbf{y}$, i.e., it is just a number rather than a function of the coordinates, Eq. (1) in higher dimensions is still an eigenproblem, and its spectrum of eigenvalues ω is the same as the spectrum of the d-dimensional quasicrystal, since the equations are identical. The physical solution is obtained by evaluating these higher-dimensional solutions at a fixed $\mathbf{y}$, say, $\mathbf{y}=0$ (where a different $\mathbf{y}$ merely corresponds to an offset in $\mathbf{x}$ as described above).

For a real, positive ε, both the physical operator and the extended operator in Eq. (1) are Hermitian and positive semidefinite, leading to many important properties such as real frequencies ω.[45]

A. Bloch's theorem and numerics for quasicrystals

Because the superspace eigenproblem is periodic, Bloch's theorem applies: the eigenfunctions $\mathbf{H}(\mathbf{x},\mathbf{y})$ can be written in the Bloch form $\mathbf{h}(\mathbf{z})e^{i\mathbf{k}\cdot\mathbf{z}}$, where $\mathbf{h}$ is a *periodic* function defined by its values in the unit cell, and $\mathbf{k}$ is the n-dimensional Bloch wave vector.[45]

Here, $\mathbf{k}$ determines the phase relationship between $\mathbf{H}$ in different unit cells of the superspace, but it does not have a simple interpretation once the solution is projected into physical space. The reason is that $\mathbf{h}$, viewed as a function of $\mathbf{x}$, is again only quasiperiodic: translation in $\mathbf{x}$ "wraps" the slice into a different portion of the unit cell, so both $\mathbf{h}$ and $e^{i\mathbf{k}\cdot\mathbf{z}}$ change simultaneously, and the latter phase cannot be easily distinguished. This prevents one from defining a useful phase or group velocity of the PQC modes.

The key point is that Bloch's theorem reduces the eigenproblem to a finite domain (the n-dimensional unit cell), rather than the infinite domain required to describe the quasicrystal solutions in physical space. This means that standard numerical methods to find the eigenvalues of differential operators are immediately applicable. For example, since the solution $\mathbf{h}$ is periodic, one can apply a plane wave expansion method[46] for $\mathbf{h}$:

$$\mathbf{h}(\mathbf{z}) = \sum_{\mathbf{G}} \tilde{\mathbf{h}}_{\mathbf{G}} e^{i\mathbf{G}\cdot\mathbf{z}}, \tag{2}$$

where the summation is over all n-dimensional reciprocal lattice vectors $\mathbf{G}$. Because the curl operations only refer to the $\mathbf{x}$ coordinates, $\nabla_{\mathbf{x}}\times\mathbf{h}$ is replaced by a summation over $\mathbf{g}_{\mathbf{x}}\times\tilde{\mathbf{h}}_{\mathbf{G}}$, where $\mathbf{g}_{\mathbf{x}}$ denotes $\mathbf{G}$ projected into X. The resulting eigenproblem for the Fourier coefficients $\tilde{\mathbf{h}}$ (once they are truncated to some wave vector cutoff) can be computed either by direct dense-matrix methods[47] or, more efficiently, by iterative methods exploiting fast Fourier transforms.[46] In the present paper, we do the former, which is easy to implement as a proof of concept, but for higher-dimensional computations, an iterative method will become necessary.

We should also remind the reader that there is a constraint $\nabla_{\mathbf{x}}\cdot\mathbf{H}=0$ on the eigenfunctions, in order to exclude unphysical solutions with static magnetic charges. In a plane wave method, this leads to a trivial constraint $(\mathbf{k}_{\mathbf{x}}+\mathbf{g}_{\mathbf{x}})\cdot\tilde{\mathbf{h}}=0$, again with $\mathbf{k}$ and $\mathbf{G}$ projected into X.

B. Spectrum of the quasicrystal

With a familiar eigenproblem arising from Bloch's theorem, such as that of a periodic physical structure, the eigen-

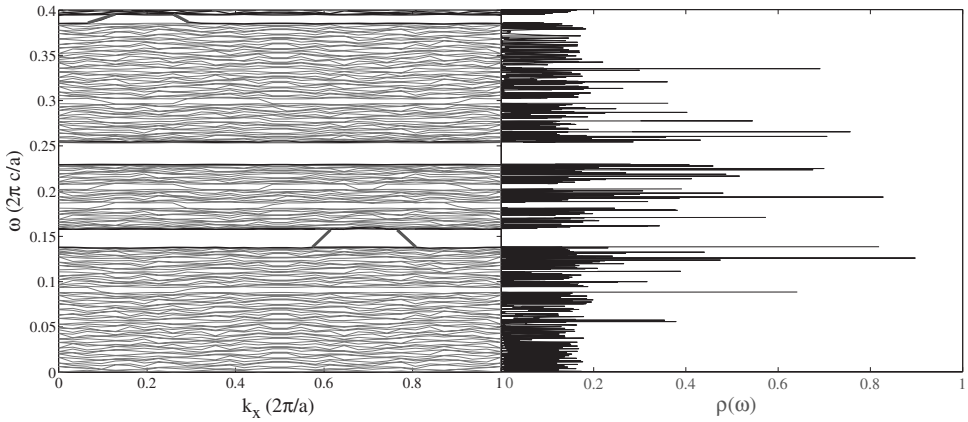

FIG. 2. Left: Frequency spectrum ω of the Fibonacci quasicrystal vs "wave vector" k_x. The blue lines indicate spurious states which arise due to finite-resolution effects (see text). Right: Corresponding density of states $\rho(\omega)$ computed using a transfer-matrix technique with a supercell of 10^4 layers.

values form a band structure: discrete bands $\omega_n(\mathbf{k})$ that are continuous functions of $\mathbf{k}$, with a finite number of bands in any given frequency range.[48] For a finite-resolution calculation, one obtains a finite number of these bands ω_n with some accuracy that increases with resolution, but even at low resolutions, the basic structure of the low-frequency bands is readily apparent. The eigenvalues of the higher-dimensional quasicrystal operator of Eq. (1), on the other hand, are quite different.

The underlying mathematical reason for the discrete band structure of a physical periodic structure is that the Bloch eigenoperator for a periodic physical lattice, $(\nabla+i\mathbf{k})\times\frac{1}{\varepsilon}(\nabla+i\mathbf{k})\times$, is the inverse of a compact integral operator corresponding to the Green's function, and hence, the spectral theorem applies.[49] Among other things, this implies that the eigenvalues at any given $\mathbf{k}$ for a finite unit cell form a discrete increasing sequence, with a finite number of eigenvalues below any finite ω. The same nice property does not hold for the operator extended to n dimensions, because along the $\mathbf{y}$ directions, we have no derivatives, only a variation of the scalar function ε. Intuitively, this means that the fields can oscillate very fast along the $\mathbf{y}$ directions without necessarily increasing ω, allowing one to have infinitely many eigenfunctions in a finite bandwidth. More mathematically, an identity operator is not compact and does not satisfy the spectral theorem,[49] and since the operator of Eq. (1) is locally the identity along the $\mathbf{y}$ directions, the same conclusion applies. This means that, when the $\mathbf{y}$ direction is included as a coordinate, it is possible to get an infinite number of bands in a finite bandwidth at a fixed $\mathbf{k}$.

In fact, as we shall see below, this is precisely what happens, and moreover, it is what *must* happen in order to reproduce the well-known properties of quasicrystal spectra. It has been shown that quasicrystal spectra can exhibit a fractal structure,[28] with infinitely many gaps (of decreasing size) in a finite bandwidth, and such a structure could not arise from an ordinary band diagram with a finite number of bands in a given bandwidth. Of course, once the unit cell is discretized for numerical computation, the number of degrees of freedom and, hence, the number of eigenvalues are finite. However, as the resolution is increased, not only do the maximum frequency and the accuracy increase as for an ordinary computation, but also the number of bands in a given bandwidth increases. Thus, as the resolution is increased, more and more of the fractal structure of the spectrum is revealed.

IV. ONE-DIMENSIONAL RESULTS

As a proof of concept implementation of cut-and-project, we construct a Fibonacci quasicrystal in Sec. IV A using the projection method described above, compute the band structure as a function of the projected wave vector k_x, and compare to a transfer-matrix calculation of the same quasicrystal structure. We also demonstrate the field visualization enabled by the projection method, both in the superspace (n dimensions) and in the physical space (d dimensions). In Sec. IV B, we demonstrate how this method can accommodate systems with defects. Finally, we explore several one-dimensional quasicrystal configurations in Sec. IV C by varying the cut angle ϕ.

A. Fibonacci quasicrystal

1. Spectrum

We solved Eq. (1) numerically using a plane wave expansion in the unit cell of the 2D superspace, as described above, for the 1D Fibonacci quasicrystal structure depicted in Fig. 1. The resulting band diagram is shown in Fig. 2(left), along with a side-by-side comparison of the local density of states in Fig. 2(right) calculated using a transfer-matrix approach with a supercell of 10^4 layers.[50] The two calculations show excellent agreement in the location of the gaps, except for one or two easily identified spurious bands inside some of the gaps, which are discussed in further detail below (Sec. IV A 3). The most important feature of Fig. 2(left) is the large number of bands even in the finite bandwidth $\omega \in [0,0.4]$, with the number of bands increasing proportional to the spatial resolution (plane wave cutoff). This is precisely the feature predicted abstractly above, in Sec. III B: at a low resolution, one sees only the largest gaps, and at higher resolutions, further details of the fractal spectrum are revealed as more and more bands appear within a given bandwidth, very different from calculations for periodic physical media. These features are illustrated in Fig. 3. The important physical quantity is not so much the band structure, since $\mathbf{k}$ has no simple physical meaning as discussed previously, but, rather, the density of states formed by projecting the band structure onto the ω axis. In this density of states, the small number of

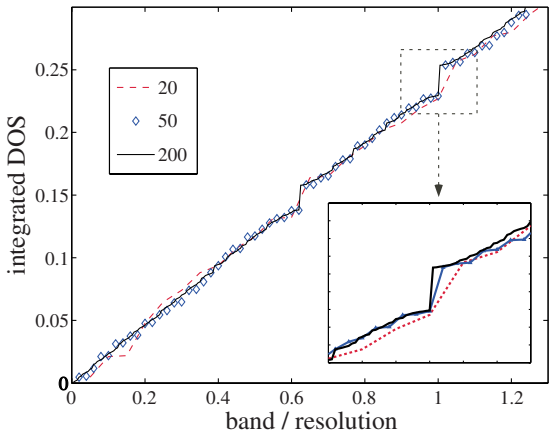

FIG. 3. (Color online) Integrated density of states (DOS) vs band index (normalized by resolution) for various resolutions. The dashed red, diamond blue, and solid black lines denote resolutions of 20, 50, and 200, respectively.

spurious bands within the gaps, which arise from the discretization as discussed below, plays no significant role: the density of states is dominated by the huge number of flat-bands (going to infinity as the resolution is increased), and the addition of one or two spurious bands is negligible.

2. Visualizing the eigenmodes in superspace

Computing the eigenmodes in the higher-dimensional superspace immediately suggests a visualization technique: instead of plotting the quasiperiodic fields as a function of the physical coordinates x by taking a slice, plot them in the two-dimensional superspace. This has the advantage of revealing the entire infinite aperiodic field pattern in a single finite plot.[34] Such plots are also used below to aid in understanding the spurious modes localized at staircased interfaces. A typical extended mode profile is shown in Fig. 4, plotted both as a function of the physical coordinate x for a large supercell and also in the unit cell of the superspace (inset). In the inset superspace plot, one can clearly see the predicted field oscillations perpendicular to the slice plane, as well as a slower oscillation rate (inversely proportional to the frequency) parallel to the slice. In the plot versus x, one can see the longer-range quasiperiodic structure that arises from how the slice wraps around the unit cell in the superspace. The factor of 3–4 long-range variations in the field amplitude are suggestive of the critically localized states (power-law decay) that one expects to see in such quasicrystals.[7,51,52]

By visualizing the bands in the higher-dimensional domain, we can demonstrate the origin of the quasicrystal band gap in an interesting way. In an ordinary photonic crystal, the gap arises because the lowest band concentrates its electric-field energy in the high-dielectric regions (due to the variational principle), while the next band (above the gap) is forced to have a nodal plane in these regions (due to orthogonality).[45] A very similar phenomenon can be observed in the quasicrystal eigenmodes when plotted in the superspace. In particular, Fig. 5 displays the electric-field

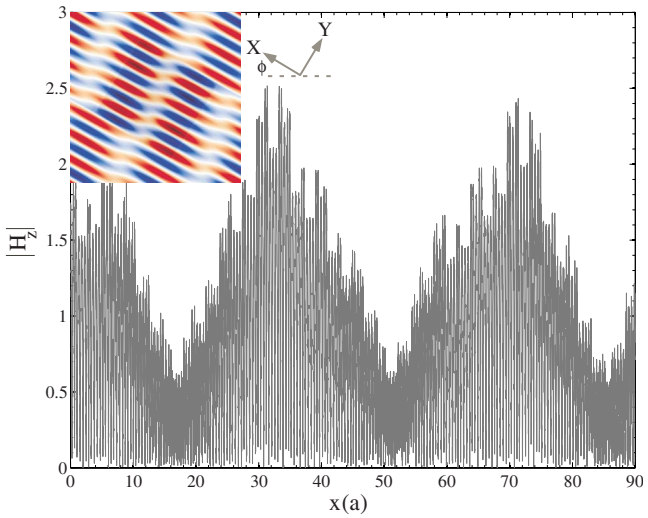

FIG. 4. (Color online) Plot of the magnetic field amplitude $|H_z|$ for a band-edge state taken along a slice of the two-dimensional superspace (in the ϕ direction). Inset: Two-dimensional superspace field profile (red/white/blue indicates positive/zero/negative amplitude).

energy distribution of the band-edge states just above and below gaps 1 and 2 of Fig. 2. Very similar to an ordinary two-dimensional photonic crystal, the bands just below the gaps are peaked in the dielectric squares, whereas the upper-edge bands have a nodal plane in these squares. If the same fields were plotted only in the physical coordinate space, the position of the peaks and nodes would vary between adjacent layers and this global pattern (including the relationship between the two gaps) might not be apparent. In contrast to a two-dimensional photonic crystal, on the other hand, the quasicrystalline field pattern has fractal oscillations in the superspace.

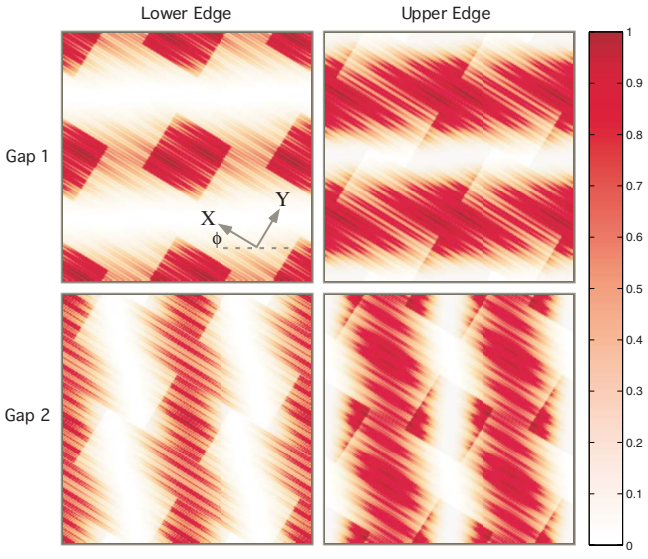

FIG. 5. (Color online) Electric field energy distribution of the band-edge states of gaps 1 and 2 in Fig. 2. Although they have a complex small-scale structure, the large-scale variation is easily understood in terms of the structure of the superspace.

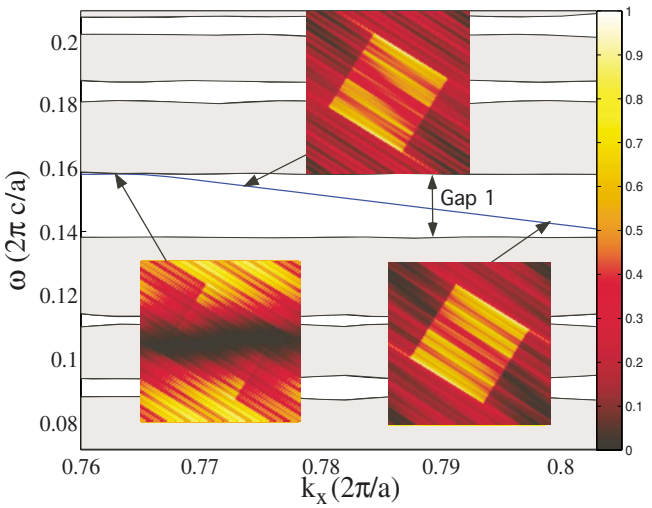

FIG. 6. (Color online) Enlarged view of the Fibonacci spectrum (Fig. 2) showing a gap with a spurious band crossing it. Insets show the magnetic field $|H_z|$ for the spurious band at various k_x—the localization of this mode around the X-parallel edges of the dielectric indicates that this is a discretization artifact.

3. Spurious modes

As the wave vector **k** varies, most of the bands in the spectrum of Fig. 2 are flat, except for certain modes (highlighted in blue) which appear to cross the band gaps relatively quickly, as shown in Fig. 6. These are the spurious modes, as explained below.

In fact, a simple argument shows that, in the limit of infinite resolution, the physical spectrum cannot depend on **k** and, hence, any strongly **k**-dependent band must be a numerical artifact. First, ω cannot depend on the components of **k** in the unphysical directions Y, because the Maxwell operator of Eq. (1) has no **y** derivatives (equivalently, any phase oscillations in **y** commute with the operator). Second, ω cannot depend on the components of **k** in the physical directions X either. The reason is that, from Bloch's theorem, **k** and **k**+**G** give the same eigensolutions for any reciprocal lattice vector **G**, and the projections of the reciprocal lattice vectors are dense in X for a quasicrystal.

These "spurious" bands that appear arise from the discretization of the dielectric interfaces parallel to the slice direction. Because the slice is at an irrational angle, it will never align precisely with a uniform grid, resulting in inevitable staircasing effects at the boundary. With ordinary electromagnetic simulations, these staircasing effects can degrade the accuracy,[53] but here the lack of derivatives perpendicular to the slice allows spurious modes to appear along these staircased edges (there is no frequency penalty to being localized perpendicular to the slice). Indeed, if one looks at the field patterns for the spurious modes as a function of $\mathbf{k}_x$ (shown in Fig. 6), one sees that the field intensity is peaked along the slice-parallel dielectric interfaces. Because they are localized to these interfaces and are, therefore, dominated by the unphysical staircasing, the spurious modes behave quite differently from the "real" solutions and are easily distinguished qualitatively and quantitatively (e.g., via their **k** dependence). Most importantly, as the resolution is increased, the number of spurious modes in a given gap does not increase like all of the other bands, because the thickness of the staircased interface region decreases proportional to the resolution. This makes the gaps in the band structure obvious: here, they are the only frequency ranges for which the number of eigenvalues does not increase with resolution. Equivalently, as noted above, the contribution of the spurious bands to the density of states is asymptotically negligible as resolution is increased.

B. Defect modes

Much of the interest in quasicrystal band gaps, similar to the analogous case of band gaps in periodic structures, centers around the possibility of localized states: by introducing a defect in the structure, e.g., by changing the thickness of a single layer, one can create exponentially localized states in the gap.[4,54] In periodic systems, because such defects break the periodicity, they necessitate a larger computational cell, or supercell, that contains many unit cells. In quasicrystal systems, once the gaps are known, on the other hand, defect states are arguably *easier* to compute than the gaps of the infinite structure, because an exponentially localized defect mode can be computed accurately with a traditional supercell and the infinite quasicrystal *per se* need not be included. Nevertheless, the superspace approach allows one to compute defect modes using the same higher-dimensional unit cell, which demonstrates the flexibility of this approach and provides an interesting (but not obviously superior) alternative to traditional supercells for defect states.

Ideally, if one had infinite spatial resolution, a defect in the crystal would be introduced as a very thin perturbation parallel to the slice direction. As the thickness of this perturbation goes to zero, it intersects the physical slice at greater and greater intervals in the physical space, corresponding to localized defects that are separated by arbitrarily large distances. In practice, of course, the thickness of the perturbation is limited by the spatial resolution, but one can still obtain defects that are very widely separated—since the associated defect modes are exponentially localized, the coupling between the defects is negligible. In other words, one effectively has a very large supercell calculation, but expressed in only the unit cell of the higher-dimensional lattice.

As an example, we changed an $\varepsilon=2.56$ layer to $\varepsilon=\varepsilon_d$ at one place in the Fibonacci quasicrystal. The corresponding superspace dielectric function is shown in Fig. 7, where the defect is introduced as a thin $(0.02a)$ strip of ε_d parallel to the slice direction. We compute the band structure as a function of the defect dielectric constant ε_d, varying it from the normal dielectric $\varepsilon_d=2.56$ up to $\varepsilon_d=11$. The thickness of the defect in the unphysical direction was fixed to be ≈ 0.02. The reason for this is that the defect layer must be greater than 1 pixel thick in the Y directions in order to avoid staircasing effects in the spectrum. The resulting eigenvalues as a function of ε_d are shown in Fig. 8 for two different spatial resolutions of 50 (blue) and 100 (red) pixels/a. When the resolution is 50, the defect is only 1 pixel thick; the discretization effects might be expected to be large, although the frequency

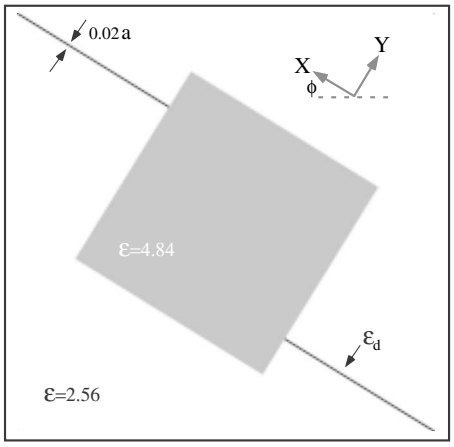

FIG. 7. Dielectric for the Fibonacci chain with $\varepsilon=2.56$ (bottom left), and a defect—an additional $\varepsilon_d=8.0$ layer; shown in gray.

is within about 2% of the higher-resolution calculation. At the higher resolution, the frequency of the mode is converging (it is within 0.3% of a resolution-200 calculation, not shown). However, at the higher resolution, there is a second, spurious mode due to the finite thickness (2 pixels) of the defect layer—this spurious mode is easily identified when the field is plotted [Fig. 9 (bottom)], because it has a sign oscillation perpendicular to the slice (which would be disallowed if we could make the slice infinitesimally thin).

The defect modes for the resolution 100 are plotted in Fig. 9 for both the real and the spurious modes versus the physical coordinate (x) and also in the superspace unit cell (insets). When plotted versus the physical coordinate x on a semilogarithmic scale, we see that the modes are exponentially localized as expected. The defect mode appears at multiple x values (every $\sim 20a$ on average) because the defect has a finite thickness—the physical slice intersects it infinitely many times (quasiperiodically), as discussed above. The spurious mode (bottom panel) is also exponentially localized; it has a sign oscillation perpendicular to the slice direction (inset) which causes it to have additional phase differences between the different defects.

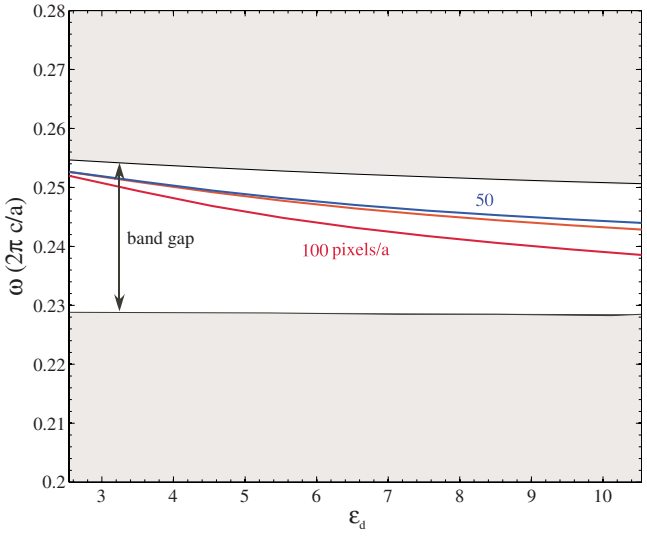

FIG. 8. (Color online) Varying the defect epsilon for resolutions 50 (blue) and 100 (red). The thickness of the defect is fixed to 0.02 lattice constants. The number of spurious modes increases with the resolution, the true defect state being the lowest of these modes.

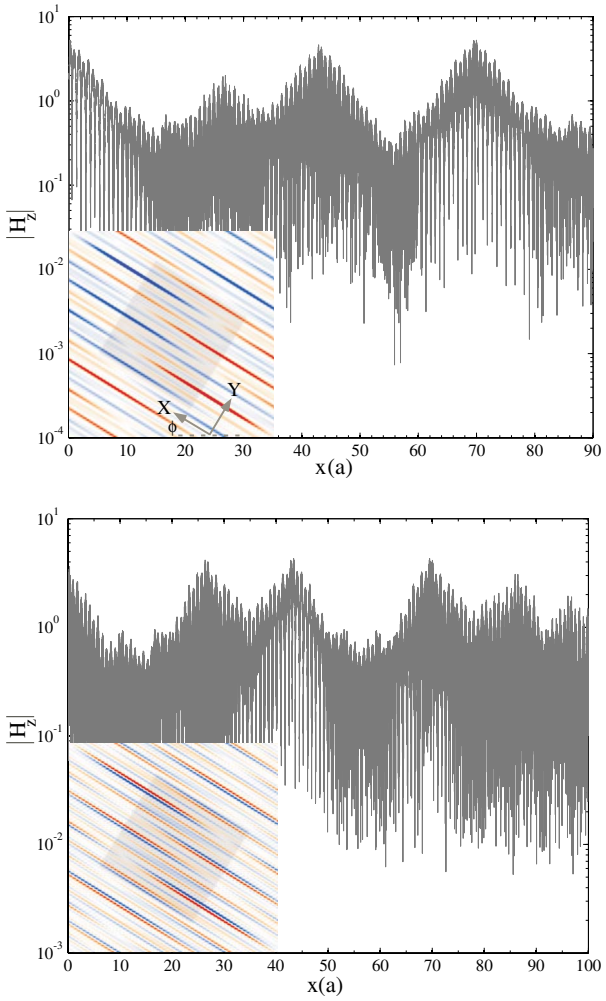

FIG. 9. (Color online) Semilogarithmic plots of the magnetic field magnitude H_z for the lowest (top) and highest (bottom) defect state for the configuration shown in Fig. 7. Insets: Two-dimensional superspace visualizations of the defect states. Note the additional node in the lower figure (corresponding to an unphysical oscillation).

Nevertheless, as emphasized above, we feel that the main advantages of the superspace approach are for studying the gaps and modes of the infinite, defect-free quasicrystal rather than for localized defect modes.

C. Continuously varying the cut angle

The cut-and-project construction of quasicrystals provides a natural way to parametrize a family of periodic and quasiperiodic structures, via the cut angle ϕ. It is interesting to observe how the spectrum and gaps then vary with ϕ.

As ϕ is varied continuously from 0° to 45°, the structures vary from period a to quasiperiodic lattices (for tan ϕ irrational) to long-period structures (tan ϕ rational with a large

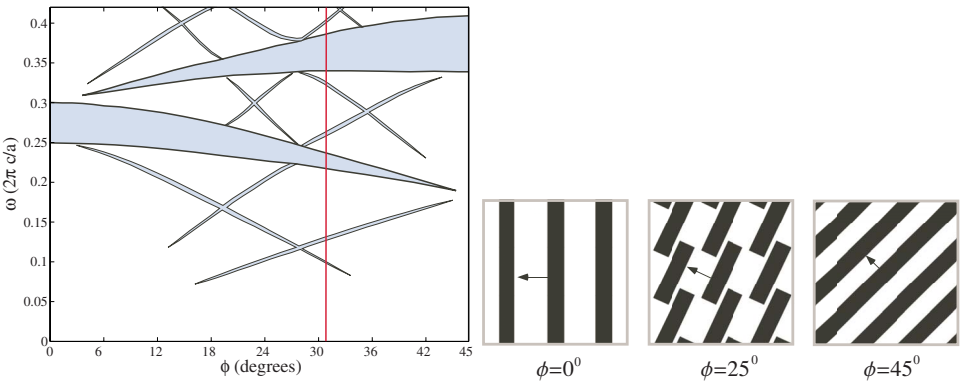

FIG. 10. (Color online) Projected band structure vs cut angle ϕ, showing different one-dimensional quasicrystal realizations. The vertical red line indicates the spectrum when the slope is the golden ratio τ (the spectra of ϕ and $\pi-\phi$ are equivalent).

denominator) to a period $a\sqrt{2}$ crystal. As we change ϕ, we rotate the objects in the unit cell, so that they are always extruded along the y direction with a length equal to the projection of the unit cell onto y $[a(\sin\phi+\cos\phi)]$, corresponding to the usual cut-and-project construction.[28] In this case, the spectrum varies continuously with ϕ, where the rational $\tan\phi$ corresponds to "rational approximants" of the nearby irrational $\tan\phi$.[29,31] For a general unit cell with a rational $\tan\phi$, the physical spectrum might depend on the slice offset **y** and, hence, different from the total superspace spectrum, but this is not the case for dielectric structures like the one here, which satisfy a "closeness" condition[29] (the edges of the dielectric rods overlap when projected onto the Y direction). This makes the structure **y** independent even for rational slices.[29] The resulting structures are shown in the bottom panel of Fig. 10 for three values of ϕ.

The corresponding photonic band gaps are shown in the top panel of Fig. 10 as a continuous function of ϕ. Only the largest gaps are shown, of course, since we are unable to resolve the fractal structure to arbitrary resolution. As might be expected, there are isolated large gaps at $\phi=0°$ and $\phi=45°$ corresponding to the simple $ABAB\ldots$ periodic structures at those angles (with period a and $a/\sqrt{2}$, respectively; the latter resulting from two layers per unit cell). The $\phi=45°$ gap is at a higher frequency because of its shorter period, but, interestingly, it is not continuously connected to the $\phi=0°$ gap.

The reason for this is that the two gaps are dominated by different superspace reciprocal lattice vectors: $(1,0)\cdot 2\pi/a$ for $\phi=0°$, and $(1,1)\cdot 2\pi/a$ for $\phi=45°$. [In fact, it is possible to calculate, to first order, the locations of the gaps using the dynamic structure factor $S(\mathbf{k},\omega)$ obtained from the projection of the superspace lattice.[55]] For intermediate angles, a number of smaller gaps open and then close. If we were able to show the spectrum with higher resolution, we would expect to see increasing numbers of these smaller gaps opening, leading to the well-known fractal structure that arises, e.g., for the Fibonacci crystal.

There is a strong similarity between the gap structure above (Fig. 10) and the well-known Hofstadter butterfly spectrum.[56] This resemblance is a consequence of the mathematical correspondence between quasiperiodic Maxwell equations and the equations of motion in Hofstadter's problem.[52] In particular, a comparison of both equations shows that the magnetic flux through the lattice in Hofstadter's problem plays precisely the same role as the slope of the cut plane $\tan\phi$ in ours, and a similar correspondence was used to experimentally reproduce Hofstadter's butterfly.[57]

V. CONCLUDING REMARKS

We have presented a numerical approach to computing the spectra of photonic quasicrystals by directly solving Maxwell's equations extended to a periodic unit cell in higher dimensions, allowing us to exploit Bloch's theorem and other attractive properties of computations for periodic structures. In doing so, we extended the conceptual approach of cut-and-project techniques, which were developed as a way to *construct* quasicrystals, into a way to *simulate* quasicrystals. Compared to traditional supercell techniques, this allows us to capture the entire infinite aperiodic quasicrystal in a single finite computational cell, albeit at only a finite resolution. In this way, the single convergence parameter of spatial resolution replaces the combination of resolution and supercell size in traditional calculations, in some sense uniformly sampling the infinite quasicrystal. The resulting computations, applied to the test case of a Fibonacci quasicrystal, display the unique features of quasicrystals in an unusual fashion, in terms of higher-dimensional band structures and visualization techniques. This technique also allows defects and variation of cut angle (continuously varying between periodic and aperiodic structures) in a straightforward way.

In future work, we plan to apply this approach to modeling higher-dimensional quasicrystal structures, such as the Penrose[30] and 2D Fibonacci tilings,[43] where computing the spectrum is currently more challenging using existing supercell techniques. To make a higher-dimensional superspace calculation practical, one must use iterative eigensolver methods[46,58] rather than the simple dense-matrix techniques employed for our test case. Iterative techniques are most efficient for computing a few eigenvalues at a time, and so it will be useful to employ iterative methods designed to compute "interior" eigenvalues,[46,58] allowing one to search directly for large gaps without computing the lower-lying modes. Alternatively, numerical techniques have been developed, based on filter-diagonalization methods, to directly extract the spectrum of many eigenvalues without computing the corresponding eigenvectors.[59]

ACKNOWLEDGMENTS

We would like to thank both L. Dal Negro and L. Levitov

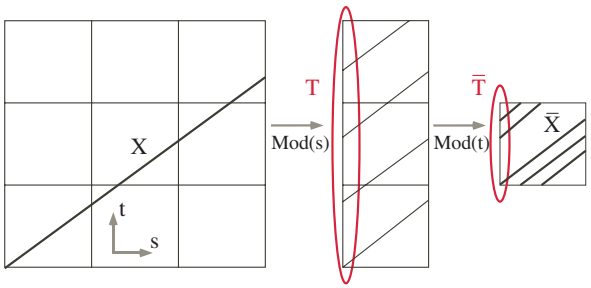

FIG. 11. (Color online) Schematic showing (left) the superspace slice X and (right) the projected slice modulo 1 into the unit cell $\bar{X}$, along with the intersection $\bar{T}$ of $\bar{X}$ with the $s=0$ hyperplane.

for useful and insightful discussions. This work was supported by the Department of Energy under Grant No. DE-FG02-97ER25308 (A.W.R.) and by the U.S. Army Research Office under Contract No. W911NF-07-D-0004 (A.P.M.).

APPENDIX

In this appendix, we give an explicit derivation of the fact that an "irrational" slice densely fills the superspace unit cell, or, rather, a definition of the necessary conditions to be an irrational slice. These concepts are widely used in the quasicrystal literature, but a precise definition seems hard to find (one commonly requires that all of the Miller indices have incommensurate ratios, but this condition is stronger than necessary).

Without loss of generality, we can consider the unit cell in the superspace $Z=\mathbb{R}^n$ to be the unit cube (related to any lattice by an affine transformation), with lattice vectors along the coordinate directions (Fig. 11). The physical slice X is d-dimensional, and it will be convenient to write the coordinates of a vector $\mathbf{z}$ as $\mathbf{z}=(s_1,\ldots,s_d,t_1,\ldots,t_{n-d})=(\mathbf{s},\mathbf{t})$. By taking every coordinate modulo 1, we can map X to a set $\bar{X}$ consisting of X's intersection with each unit cell. We wish to show necessary and sufficient conditions for $\bar{X}$ to densely fill the unit cell.

Assuming that the slice is not orthogonal to any of the coordinate axes (as, otherwise, it would clearly not densely fill the unit cell), we can parametrize the points $\mathbf{z}$ of X so that the last $n-d$ coordinates $(t_1,\ldots,t_{n-d})$ are written as a linear function $\mathbf{t}(s_1,\ldots s_d)\equiv\mathbf{t}(\mathbf{s})$ of the first d coordinates.

Consider the set T in $\mathbb{R}^{n-d}$ formed by the $\mathbf{t}(\mathbf{s})$ coordinates of X when the components of $\mathbf{s}$ take on integer values. This is a subset of X, and the corresponding set $\bar{T}$ formed by taking $\mathbf{t}\in T$ modulo 1 is a subset of $\bar{X}$. The key fact is that $\bar{X}$ is dense in the n-dimensional unit cell if and only if $\bar{T}$ is dense in the $(n-d)$-dimensional unit cell, and this is the case that we will analyze. This equivalence follows from the fact that $\bar{X}$ is simply $\bar{T}$ translated continuously along the slice directions (every point in $\bar{X}$ is related to a point in $\bar{T}$ by a simple projection). The set T is a lattice in $\mathbb{R}^{n-d}$ consisting of all integer linear combinations of the basis vectors $\mathbf{t}_k=\mathbf{t}(s_j=\delta_{jk})$, since $\mathbf{t}(\mathbf{s})$ is a linear function.

For each basis vector $\mathbf{t}_k$, it is a well-known fact[60] that if it consists of m incommensurate irrational components, the set of integer multiples $\ell\mathbf{t}_k$ modulo 1 will densely fill an m-dimensional slice of the unit cell. More precisely, write $\mathbf{t}_k=\Sigma_{j=1,\ldots,m_k}\alpha_k^j\mathbf{b}_k^j+\mathbf{q}_k$, where the $\mathbf{b}_k^j$ and $\mathbf{q}_k$ have purely rational components and the $\{\alpha_j\}$ are incommensurate irrational numbers, and m_k is, therefore, the number of incommensurate irrational components of $\mathbf{t}_k$. Then the set of integer multiples of $\mathbf{t}_k$ modulo 1 densely fills an m_k-dimensional slice of the unit cell of $\mathbb{R}^{n-d}$. The basis vectors of this slice are precisely the vectors $\mathbf{b}_k^j$, which are rational and, therefore, commensurate with the basis vectors of $\mathbb{R}^{n-d}$, while the vector $\mathbf{q}_k$ is simply a rational shift. This slice, therefore, cuts the unit cell of $\mathbb{R}^{n-d}$ a finite number of times.

The set $\bar{T}$ is then obtained as the direct sum of these dense slices for all $n-d$ vectors $\mathbf{t}_k$. This is then dense if and only if the set of vectors $\{\mathbf{b}_k^j\}_{k=1,\ldots,d}^{j=1,\ldots,m_k}$ spans $\mathbb{R}^{n-d}$. In other words, an irrational slice, which densely fills the unit cell, is one in which there are $n-d$ independent incommensurate slice components as defined above.

*alexrod7@mit.edu

[1] M. Kohmoto, B. Sutherland, and K. Iguchi, Phys. Rev. Lett. **58**, 2436 (1987).
[2] W. Gellermann, M. Kohmoto, B. Sutherland, and P. C. Taylor, Phys. Rev. Lett. **72**, 633 (1994).
[3] Y. S. Chan, C. T. Chan, and Z. Y. Liu, Phys. Rev. Lett. **80**, 956 (1998).
[4] S. S. M. Cheng, L.-M. Li, C. T. Chan, and Z. Q. Zhang, Phys. Rev. B **59**, 4091 (1999).
[5] M. E. Zoorob, M. D. B. Charlton, G. J. Parker, J. J. Baumberg, and M. C. Netti, Mater. Sci. Eng., B **74**, 168 (2000).
[6] M. E. Zoorob, M. D. Charlton, G. J. Parker, J. J. Baumberg, and M. C. Netti, Nature (London) **404**, 740 (2000).
[7] L. Dal Negro, C. J. Oton, Z. Gaburro, L. Pavesi, P. Johnson, A. Lagendijk, R. Righini, M. Colocci, and D. S. Wiersma, Phys. Rev. Lett. **90**, 055501 (2003).
[8] Y. Wang, C. Bingying, and D. Zhang, J. Phys.: Condens. Matter **15**, 7675 (2003).
[9] P. Xie, Z.-Q. Zhang, and X. Zhang, Phys. Rev. E **67**, 026607 (2003).
[10] M. Notomi, H. Suzuki, T. Tamamura, and K. Edagawa, Phys. Rev. Lett. **92**, 123906 (2004).
[11] A. Della Villa, S. Enoch, G. Tayeb, V. Pierro, V. Galdi, and F. Capolino, Phys. Rev. Lett. **94**, 183903 (2005).
[12] Z. Feng, X. Zhang, Y. Wang, Z.-Y. Li, B. Cheng, and D.-Z. Zhang, Phys. Rev. Lett. **94**, 247402 (2005).
[13] S.-K. Kim, J.-H. Lee, S.-H. Kim, I.-K. Hwang, and Y.-H. Lee, Appl. Phys. Lett. **86**, 031101 (2005).
[14] R. Lifshitz, A. Arie, and A. Bahabad, Phys. Rev. Lett. **95**, 133901 (2005).

[15] J. Romero-Vivas, D. N. Chigrin, A. V. Lavrinenko, and C. M. Sotomayor Torres, Phys. Status Solidi A **202**, 997 (2005).
[16] D. S. Wiersma, R. Sapienza, S. Mujumdar, M. Colocci, M. Ghulinyan, and L. Pavesi, J. Opt. A, Pure Appl. Opt. **7**, S190 (2005).
[17] A. Della Villa, S. Enoch, G. Tayeb, V. Pierro, and V. Galdi, Opt. Express **14**, 10021 (2006).
[18] B. Freedman, G. Bartal, M. Segev, R. Lifshitz, D. N. Christodoulides, and J. W. Fleischer, Nature (London) **440**, 1166 (2006).
[19] R. C. Gauthier and K. Mnaymneh, Opt. Commun. **264**, 78 (2006).
[20] G. J. Parker, M. D. B. Charlton, M. E. Zoorob, J. J. Baumberg, M. C. Netti, and T. Lee, Philos. Trans. R. Soc. London, Ser. A **364**, 189 (2006).
[21] Z. S. Zhang, B. Zhang, J. Xu, Z. J. Yang, Z. X. Qin, T. J. Yu, and D. P. Yu, Appl. Phys. Lett. **88**, 171103 (2006).
[22] J. Y. Zhang, H. L. Tam, W. H. Wong, Y. B. Pun, J. B. Xia, and K. W. Cheah, Solid State Commun. **138**, 247 (2006).
[23] K. Mnaymneh and R. C. Gauthier, Opt. Express **15**, 5089 (2007).
[24] M. A. Kaliteevski, S. Brand, R. A. Abram, T. F. Krauss, P. Millar, and R. De La Rue, J. Phys.: Condens. Matter **13**, 10459 (2001).
[25] X. Zhang, Z.-Q. Zhang, and C. T. Chan, Phys. Rev. B **63**, 081105(R) (2001).
[26] M. Hase, H. Miyazaki, M. Egashira, N. Shinya, K. M. Kojima, and S. I. Uchida, Phys. Rev. B **66**, 214205 (2002).
[27] M. Maldovan and E. L. Thomas, Nat. Mater. **3**, 593 (2004).
[28] C. Janot, *Quasicrystals* (Clarendon, Oxford, 1992).
[29] *Physical Properties of Quasicrystals*, edited by W. Steurer and T. Haibach (Springer, New York, 1999), Chap. 2.
[30] *Quasicrystals*, edited by J. B. Suck, M. Schreiber, and P. Hsussler (Springer, New York, 2004), Chap. 2.
[31] K. Wang, S. David, A. Chelnokov, and J. M. Lourtioz, J. Mod. Opt. **50**, 2095 (2003b).
[32] W. Man, M. Megens, P. J. Steinhardt, and P. M. Chaikin, Nature (London) **436**, 993 (2005).
[33] A. Ledermann, L. Cademartiri, M. Hermatschweiler, C. Toninelli, G. A. Ozin, D. S. Weirsma, M. Wegener, and G. V. Freymann, Nat. Mater. **5**, 942 (2006).
[34] C. de Lange and T. Janssen, Phys. Rev. B **28**, 195 (1983).
[35] J. P. Lu and J. L. Birman, Phys. Rev. B **36**, 4471 (1987).
[36] C. Godreche and J. M. Luck, Phys. Rev. B **45**, 176 (1992).
[37] X. Q. Huang, S. S. Jiang, R. W. Peng, and A. Hu, Phys. Rev. B **63**, 245104 (2001).
[38] R. C. Gauthier and K. Mnaymueh, Opt. Express **13**, 1985 (2005).
[39] M. A. Kaliteevski, S. Brand, R. A. Abram, T. F. Krauss, R. M. De La Rue, and P. Millar, J. Mod. Opt. **47**, 1771 (2000).
[40] A. Della Villa, V. Galdi, F. Capolino, V. Pierro, S. Enoch, and G. Tayeb, IEEE Antennas Wireless Propag. Lett. **5**, 331 (2006).
[41] W. Steurer and D. Sutter-Widmer, J. Phys. D **40**, R229 (2007).
[42] E. S. Zijlstra and T. Janssen, Europhys. Lett. **52**, 578 (2000).
[43] R. Lifshitz, J. Alloys Compd. **342**, 186 (2000).
[44] L. Dal Negro, M. Stolfi, Y. Yi, J. Michel, X. Duan, L. C. Kimerling, J. LeBlanc, and J. Haavisto, Appl. Phys. Lett. **84**, 5186 (2004).
[45] J. D. Joannopoulos, R. D. Meade, and J. N. Winn, *Photonic Crystals: Molding the Flow of Light* (Princeton University Press, Princeton, NJ, 1995).
[46] S. G. Johnson and J. D. Joannopoulos, Opt. Express **8**, 173 (2001).
[47] G. H. Golub and C. F. Van Loan, *Matrix Computations*, 3rd ed. (The Johns Hopkins University Press, Baltimore, MD, 1996).
[48] *Mathematical Modeling in Optical Science*, edited by G. Bao, L. Cowsar, and W. Masters, Frontiers in Applied Mathematics, Vol. 22 (SIAM, Philadelphia, 2001), Chap. 7.
[49] I. Gohberg, S. Goldberg, and M. A. Kaashoek, *Basic Classes of Linear Operators* (Birkhäuser, Basel, 2000).
[50] J. Li, D. Zhao, and Z. Liu, Phys. Lett. A **332**, 461 (2004).
[51] M. Kohmoto, L. P. Kadanoff, and C. Tang, Phys. Rev. Lett. **50**, 1870 (1983).
[52] S. Ostlund, R. Pandit, D. Rand, H. J. Schellnhuber, and E. D. Siggia, Phys. Rev. Lett. **50**, 1873 (1983).
[53] A. Farjadpour, D. Roundy, A. Rodriguez, M. Ibanescu, P. Bermel, J. Burr, J. D. Joannopoulos, and S. G. Johnson, Opt. Lett. **31**, 2972 (2006).
[54] M. Bayinding, E. Cubukcu, I. Bulu, and E. Ozbay, Europhys. Lett. **56**, 41 (2001).
[55] M. Quilichini, Rev. Mod. Phys. **69**, 277 (1997).
[56] D. Hofstadter, Phys. Rev. B **14**, 2239 (1976).
[57] U. Kuhl and H. Stockmann, Phys. Rev. Lett. **80**, 3232 (1998).
[58] Z. Bai, J. Demmel, J. Dongarra, A. Ruhe, and H. Van Der Vorst, *Templates for the Solution of Algebraic Eigenvalue Problems: A Practical Guide* (SIAM, Philadelphia, 2000).
[59] V. A. Mandelshtam and A. Neumaier, J. Theor. Comput. Chem. **1**, 1 (2002).
[60] E. Ott, *Chaos in Dynamical Systems*, 2nd ed. (Cambridge University Press, Cambridge, England, 2002).